Materials Advances

ELECTRONIC SUPPLEMENTARY INFORMATION

A multilayered supramolecular chelate of diclofenac-appended Ag^{I}-hydrazide as efficient anti-inflammatory, anticancer, and nanometal dispersing material, in comparison to analogous Zn^{II}-hydrazide

Qurrat-ul-Ain,*[a] Sammer Yousuf,[b] Summaiyah Bibi,[a] Irum Hamid,[a] Shazia Shah,[a] and Sumaira Khurshid [c]

[a] *Department of Chemistry, University of Karachi, Karachi 75270, Pakistan.*
[b] *H.E.J. Research Institute of Chemistry, International Center for Chemical and Biological Sciences, University of Karachi, Karachi 75270, Pakistan.*
[c] *Department of Chemistry, Federal Urdu University of Arts, Science and Technology, Gulshan-e-Iqbal Campus, Karachi-75300, Pakistan.*
Corresponding author Email: qurrat_chem@uok.edu.pk

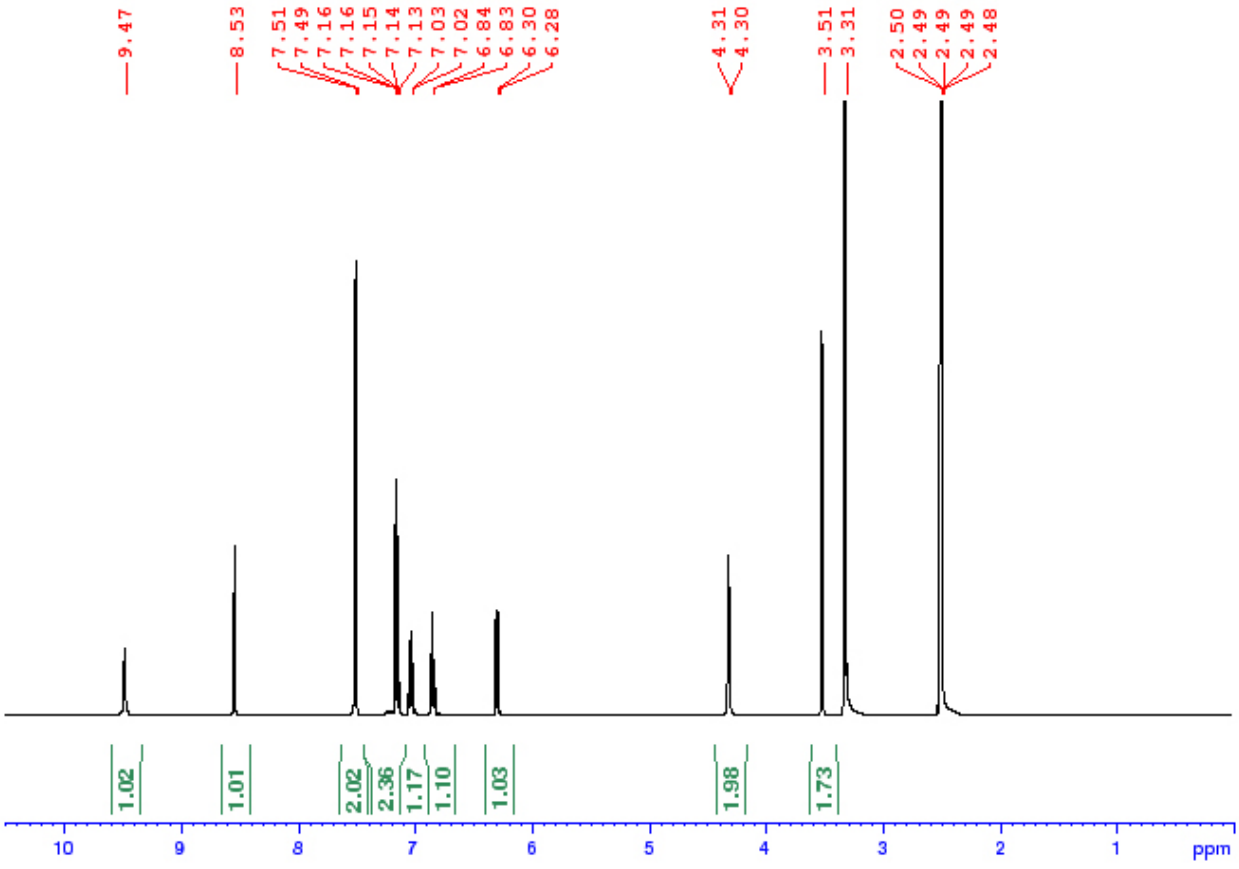

Fig. S1 ^{1}H NMR spectrum of **dh** ligand in fresh DMSO solution at 500 MHz.

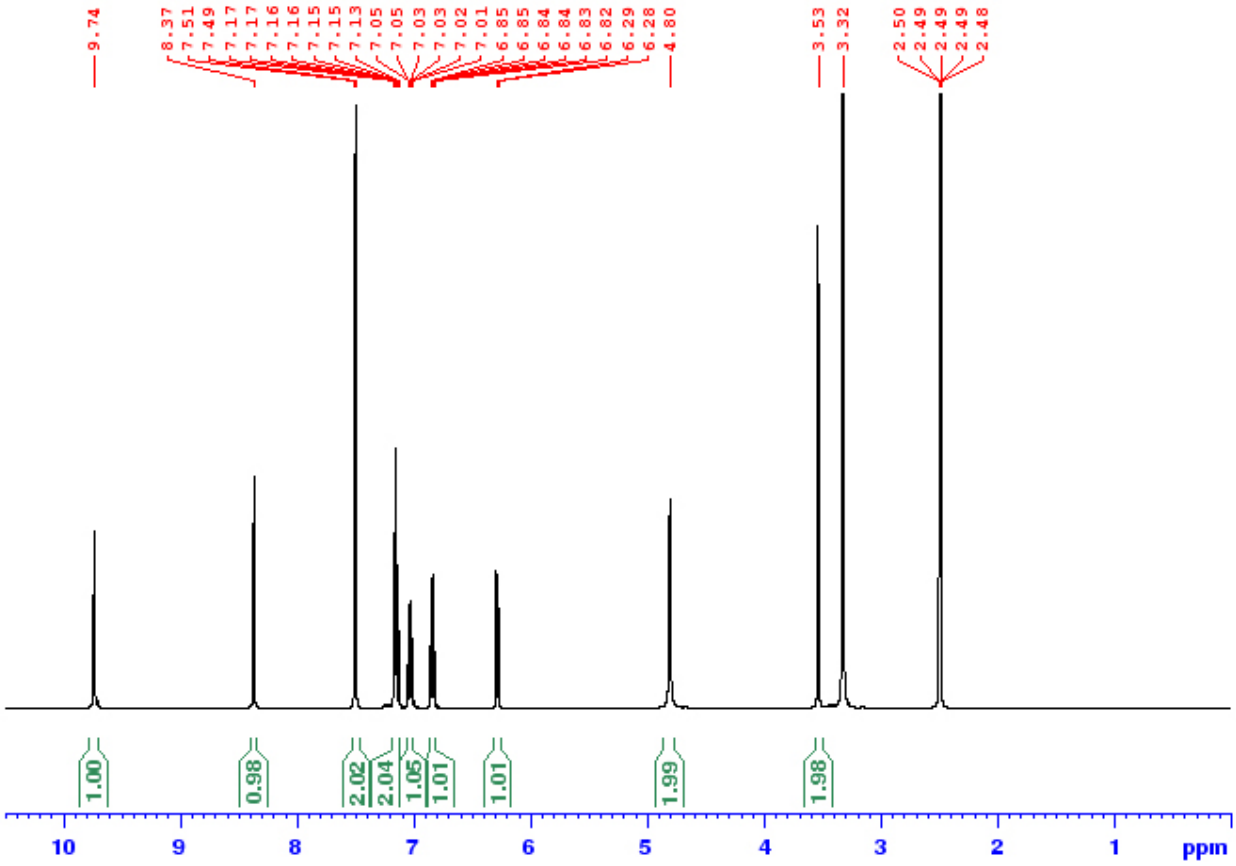

Fig. S2 ^{1}H NMR spectrum of complex **1** in fresh DMSO solution at 500 MHz.

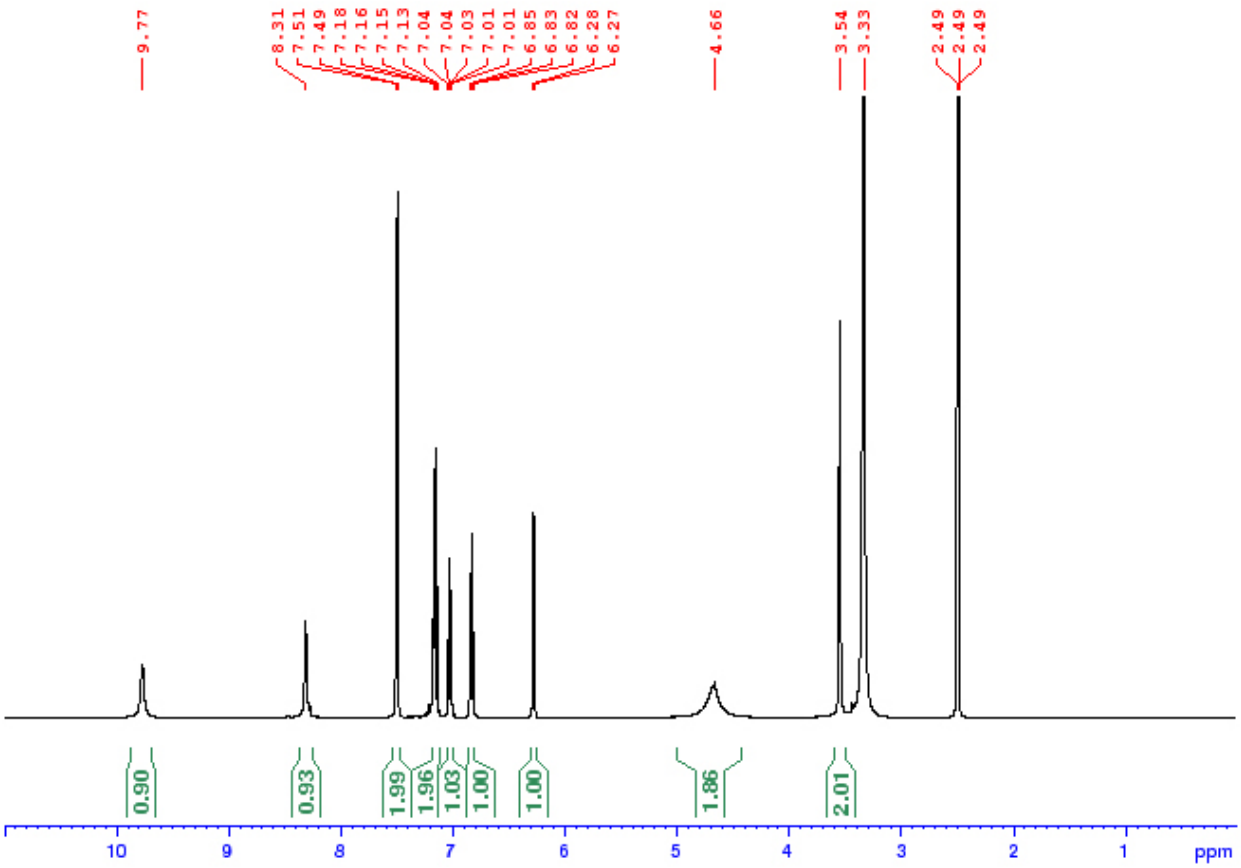

Fig. S3 ^{1}H NMR spectrum of complex **2** in fresh DMSO solution at 500 MHz.

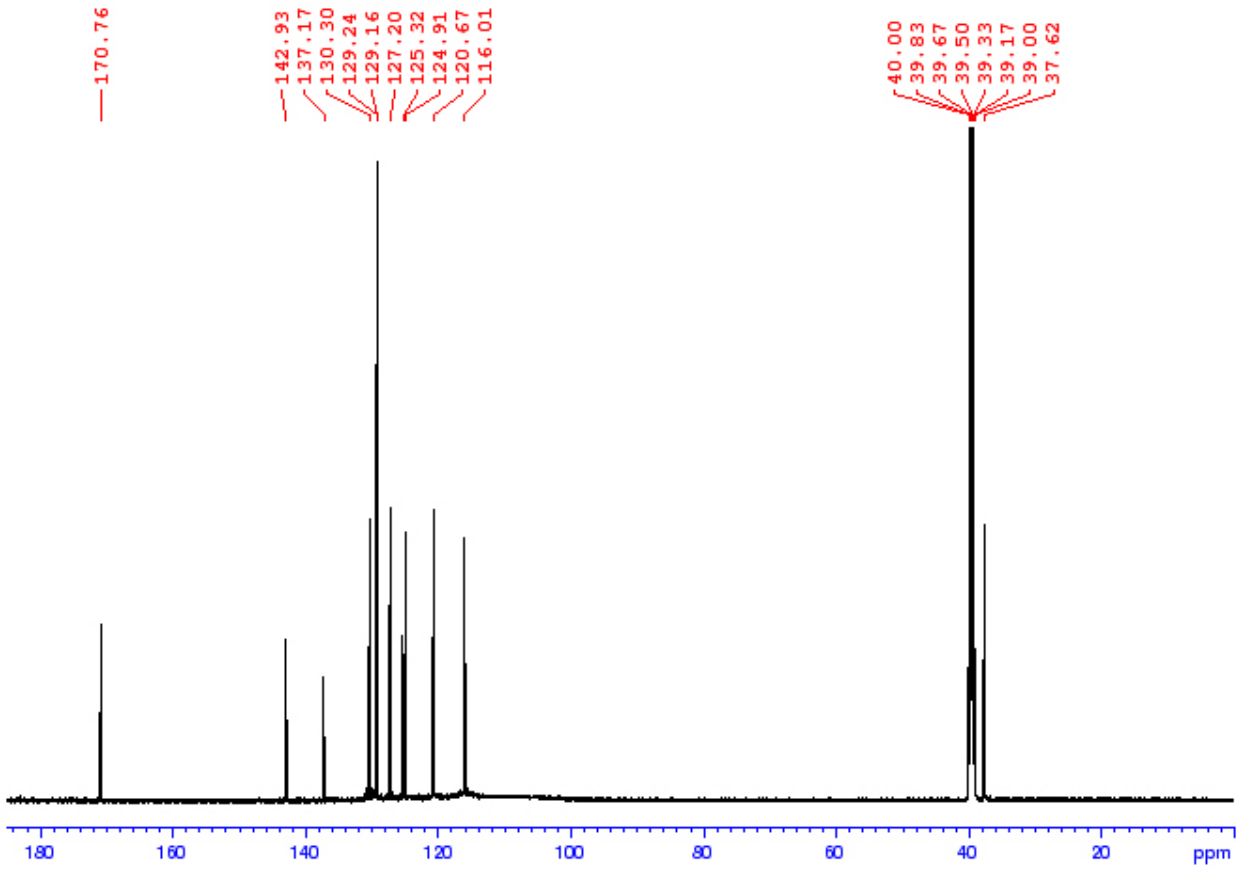

Fig. S4 $^{13}C\{^{1}H\}$ NMR spectrum of **dh** ligand in fresh DMSO solution at 125 MHz.

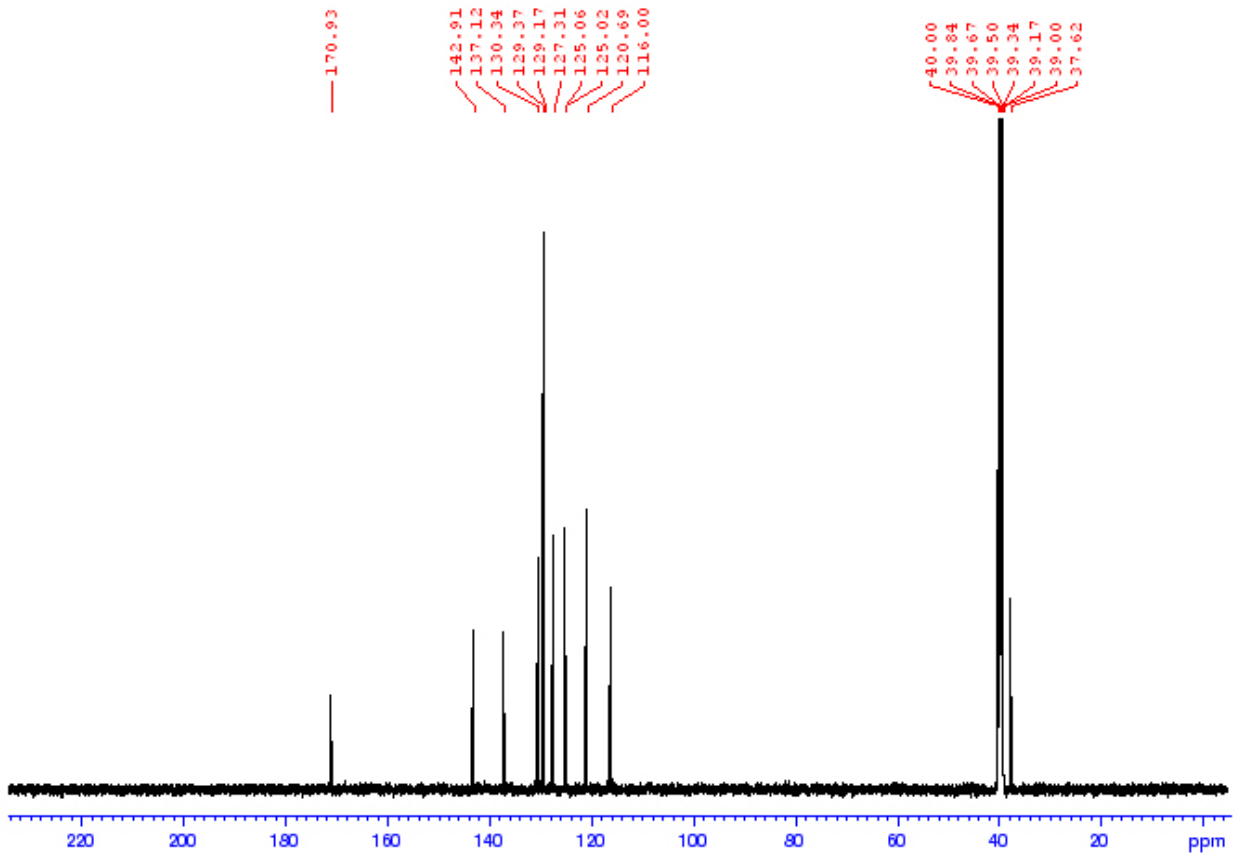

Fig. S5 $^{13}C\{^{1}H\}$ NMR spectrum of complex **1** in fresh DMSO solution at 125 MHz.

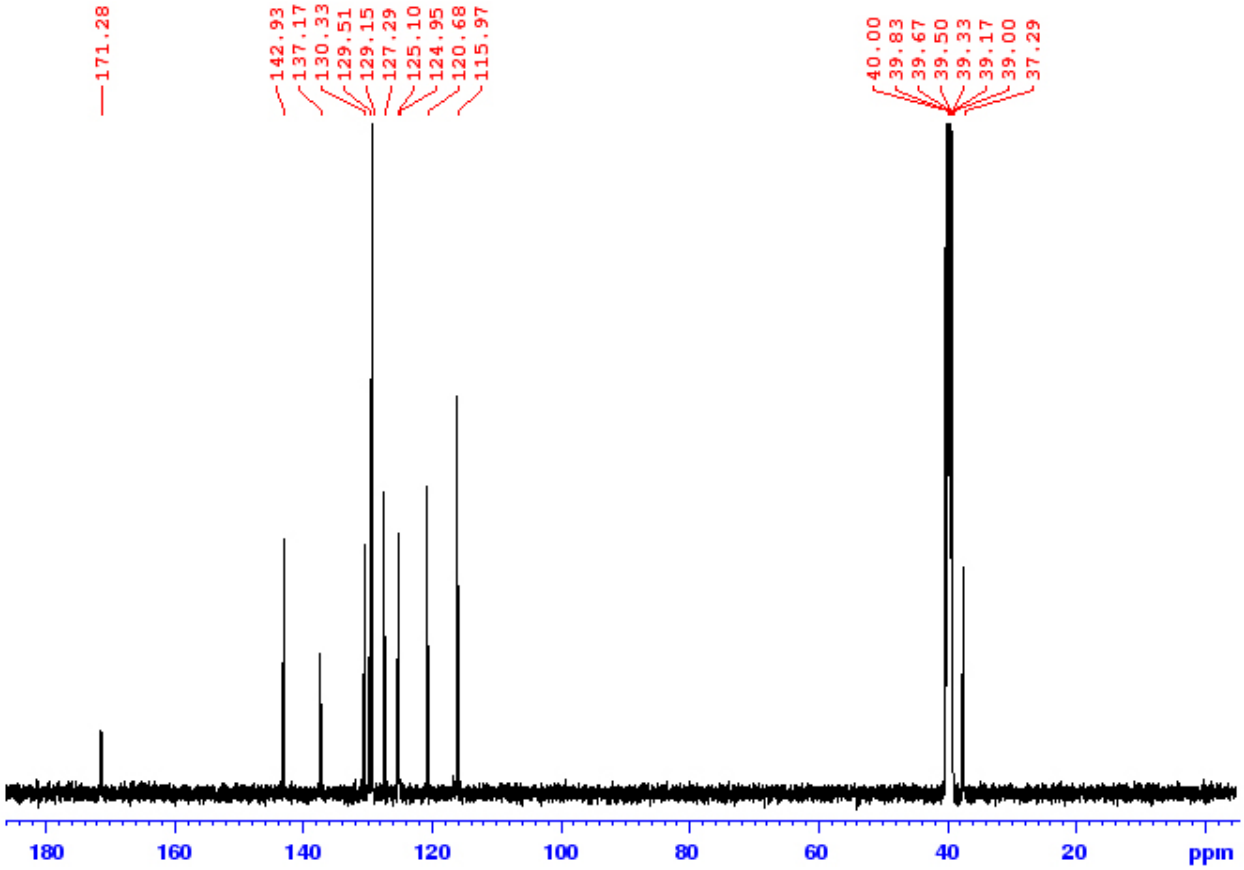

Fig. S6 $^{13}C\{^{1}H\}$ NMR spectrum of complex **2** in fresh DMSO solution at 125 MHz.

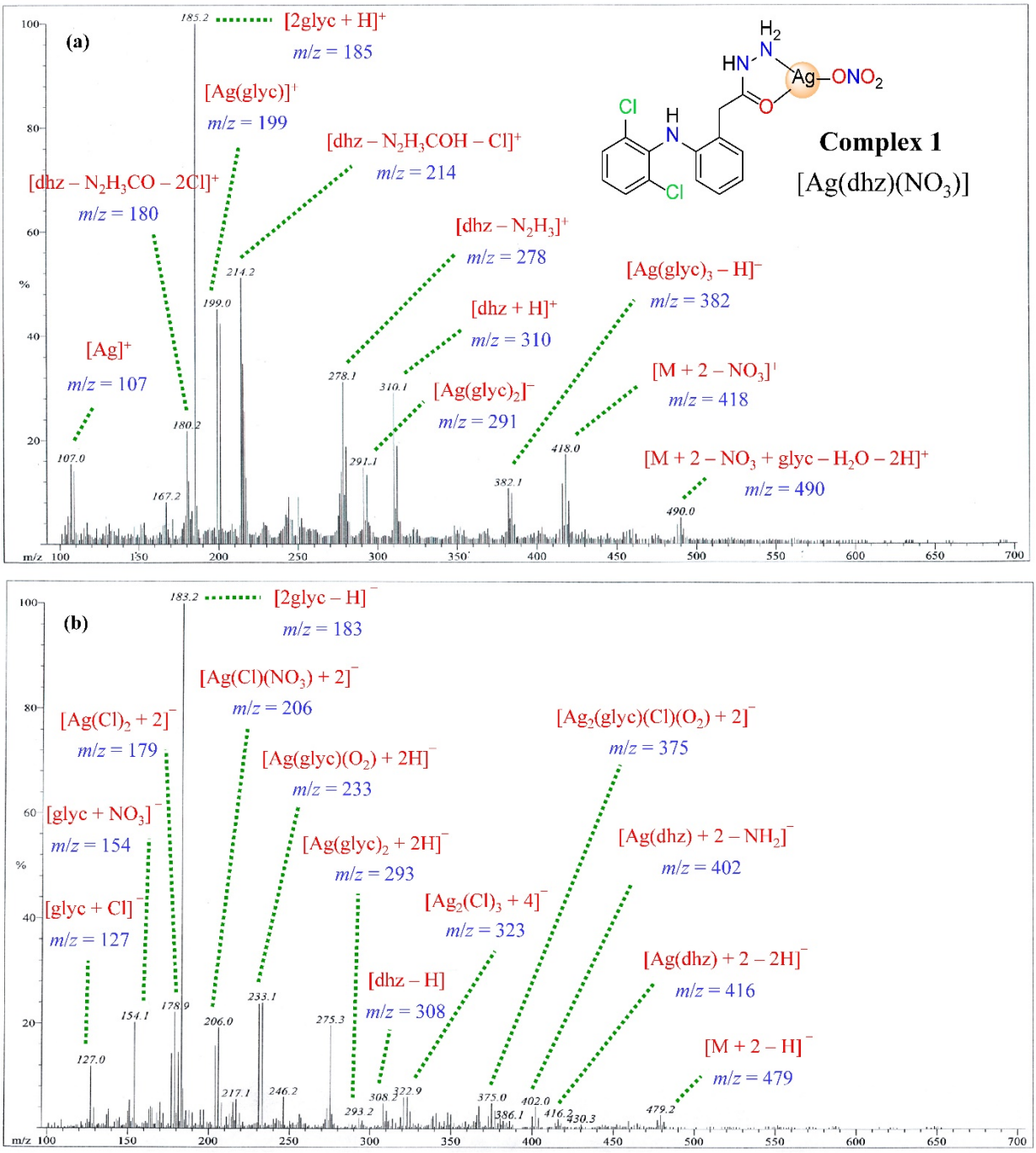

Fig. S7 FAB-mass spectrum of complex **1** in (a) positive ion and (b) negative ion modes with glycerol/DMSO matrix.

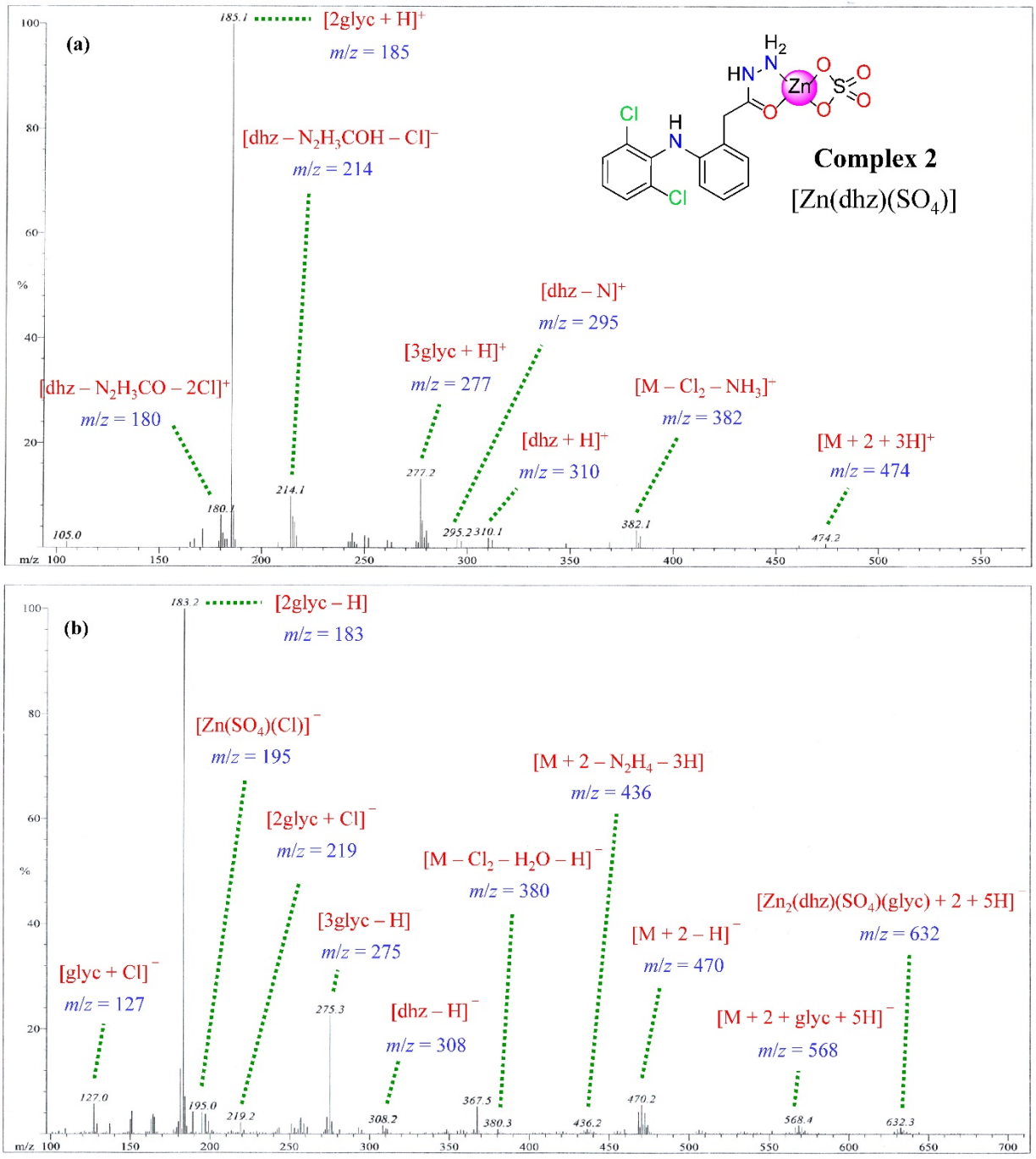

Fig. S8 FAB-mass spectrum of complex **2** in (a) positive ion and (b) negative ion modes with glycerol/DMSO matrix.

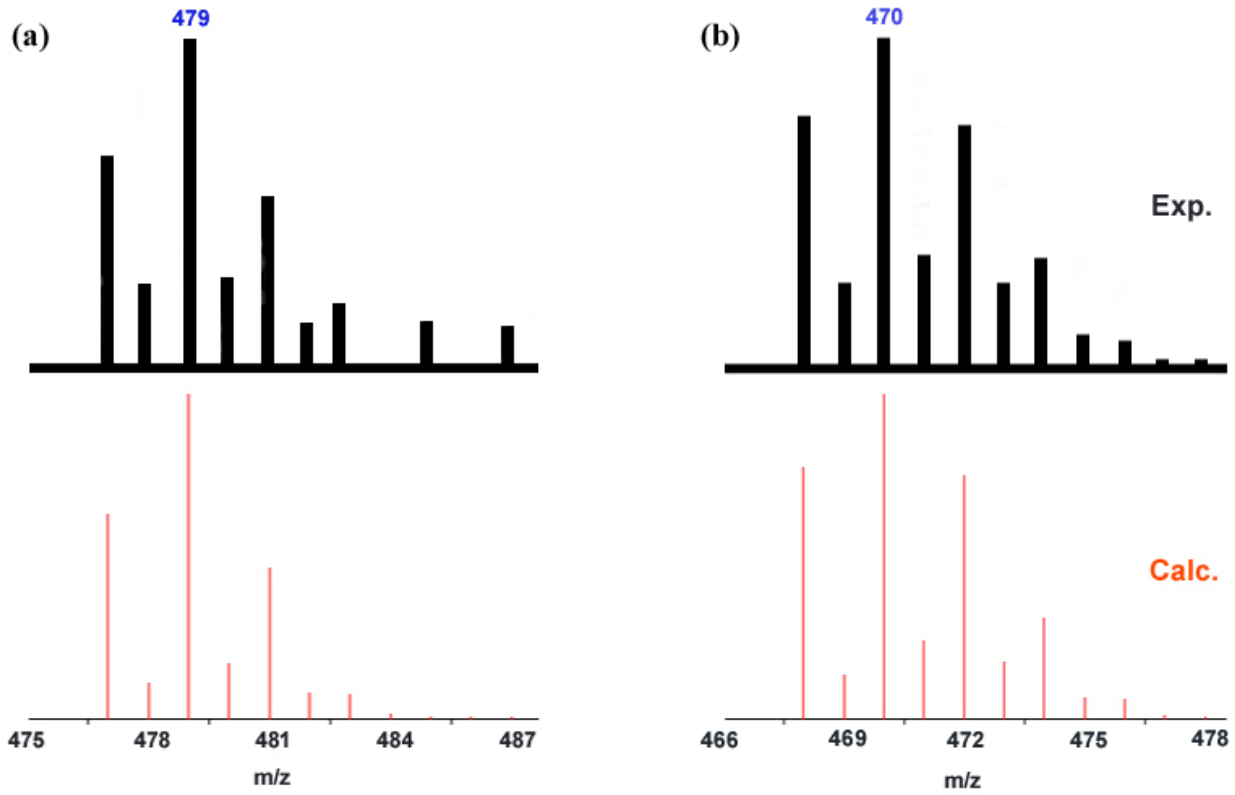

Fig. S9 FAB-mass (negative mode) spectral isotopic distribution pattern of complex **1** (a) and complex **2** (b) molecular anions $[M + 2 - H]^-$ (top/black = experimental, bottom/red = simulated).

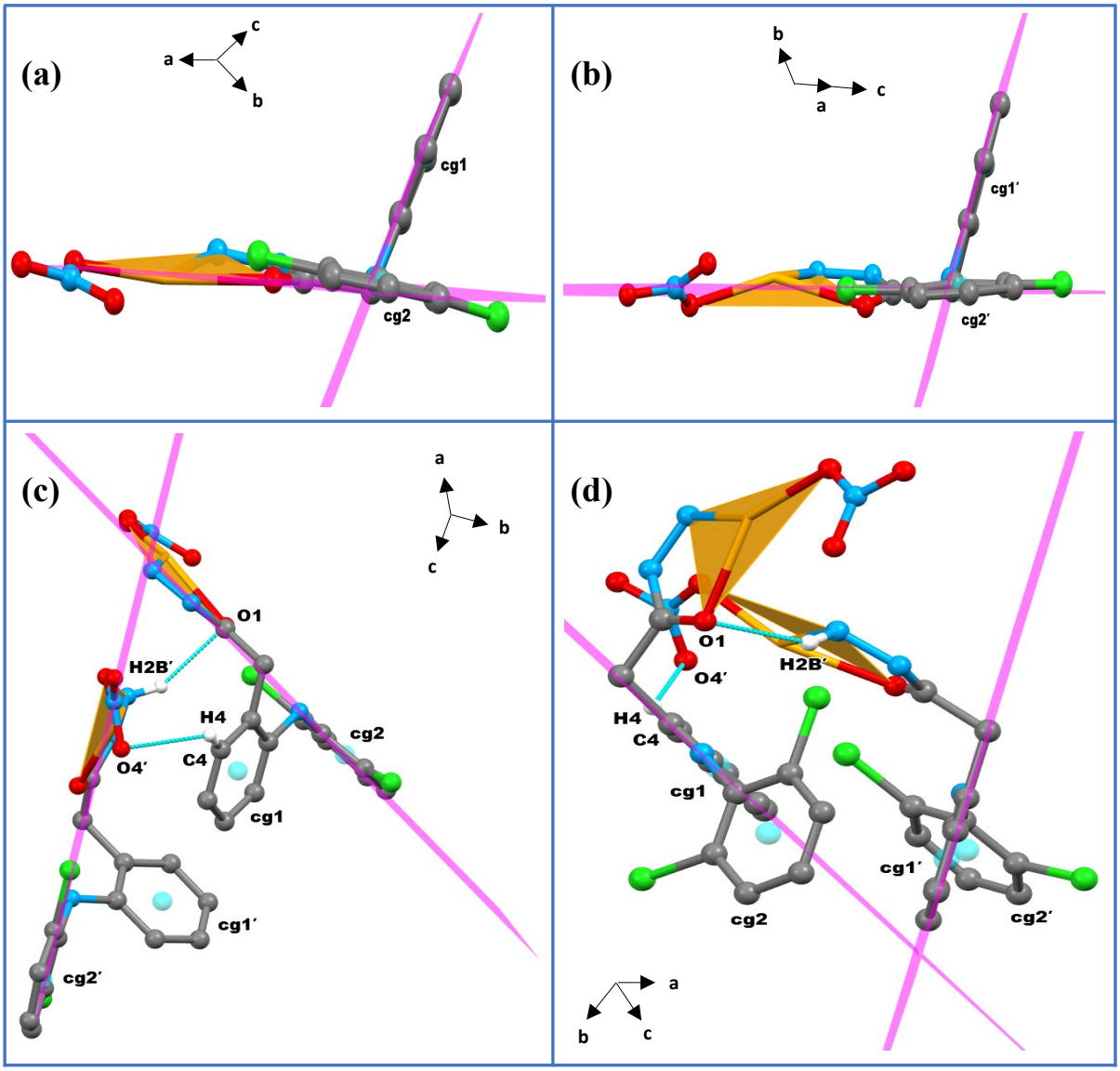

Fig. S10 Perspective view of directionality of fitted crossing planes for complex **1**: (a) cg2/trigonal-Ag1-coordination plane of molecule A crossing its cg1 plane (65.5°), (b) cg2′/trigonal-Ag1′-coordination plane of molecule A′ crossing its cg1′ plane (70.9°), (c) cg2/Ag1-coordination plane of A crossing (56.7°) the cg2′/Ag1′-coordination plane of A′, interlinked by one C-H···O and one N-H···O interaction in the asymmetric unit, and (d) cg1 plane of A crossing (58.4°) the cg1′ plane of A′ in the asymmetric unit.

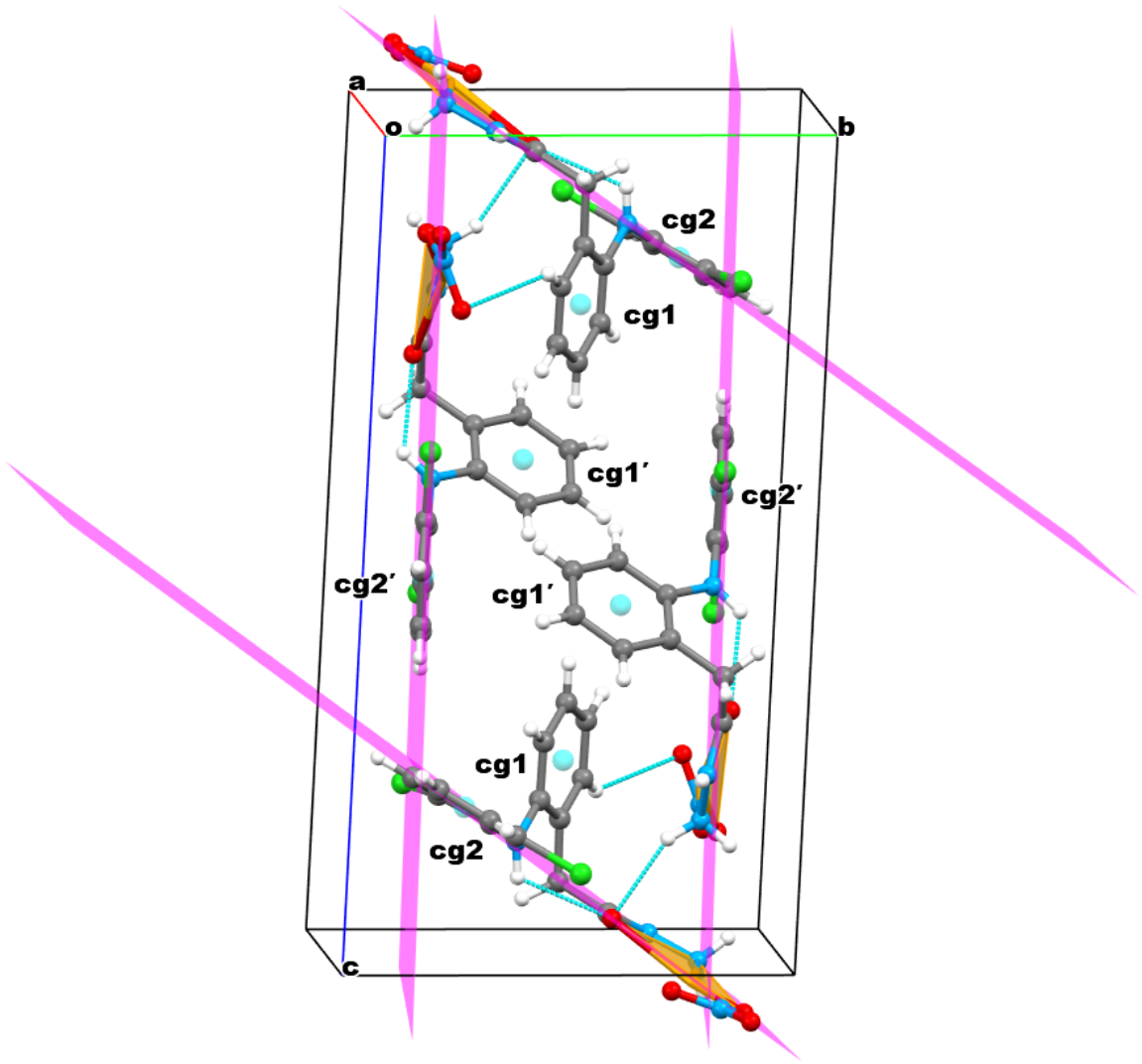

Fig. S11 Unit cell diagram of complex **1** along *a*-axis displaying hydrogen bond linkages within asymmetric units (turquoise dashed lines), along with perspective view of two sets of parallel mean molecular planes (fitted for each molecule excluding cg1/cg1′): Set 1 from two A (crossing the *ab*-plane) and set 2 from two A′ (parallel to *ac*-plane), both sets are crossing each other and making a parallelogram with central hydrophobic clustering.

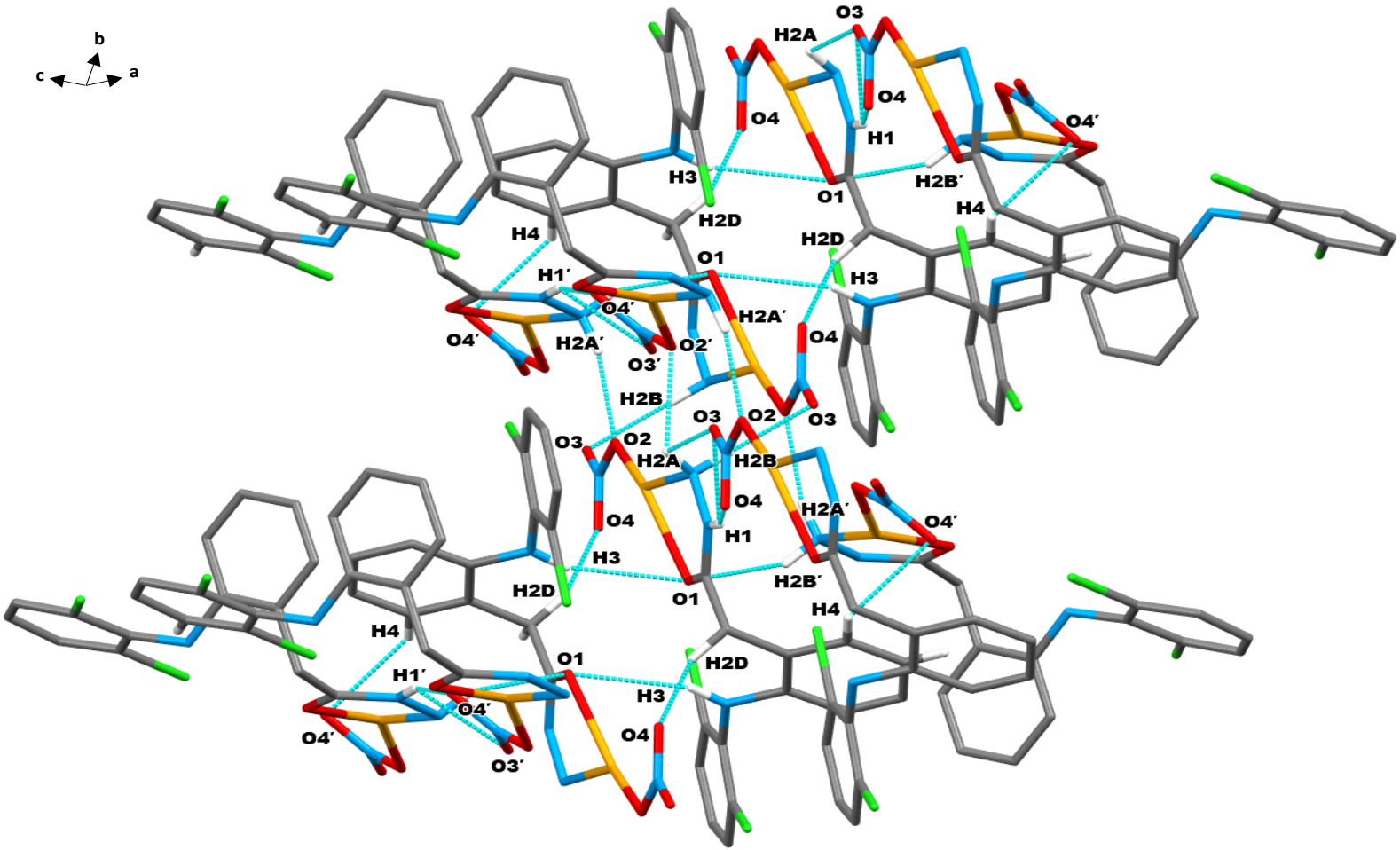

Fig. S12 Intermolecular N-H···O/C-H···O hydrogen bond interactions (turquoise dashed lines) in complex **1** in all three (*a*/*b*/*c*) directions, important for 3D network stabilization. Other hydrogen atoms are omitted for clarity.

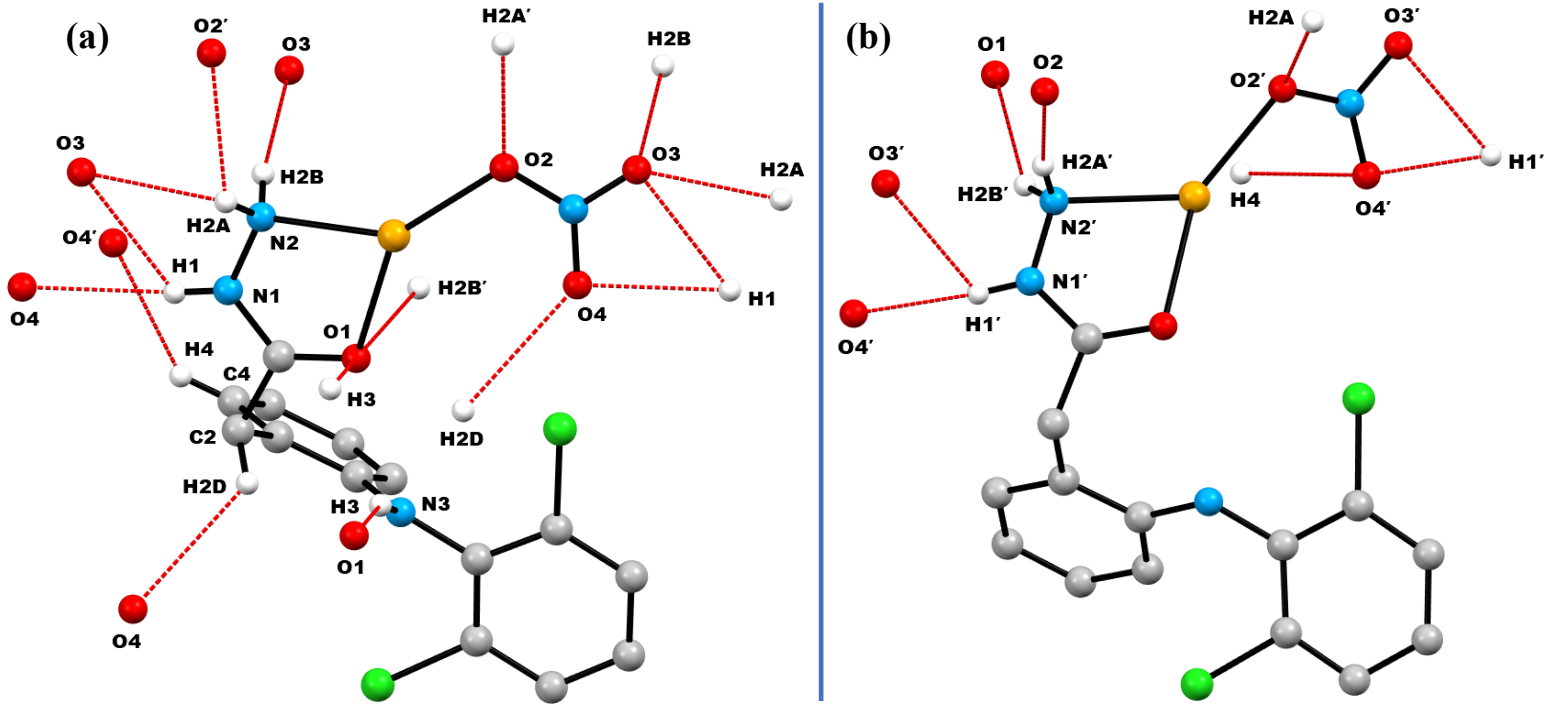

Fig. S13 All possible intermolecular donor and acceptor hydrogen bond interactions as hanging contacts (red dashed lines) generated by two independent molecules (a) A and (b) A′ of complex **1**. The full structure of interacting molecules around the central molecule and non-interacting hydrogens are not shown for clarity.

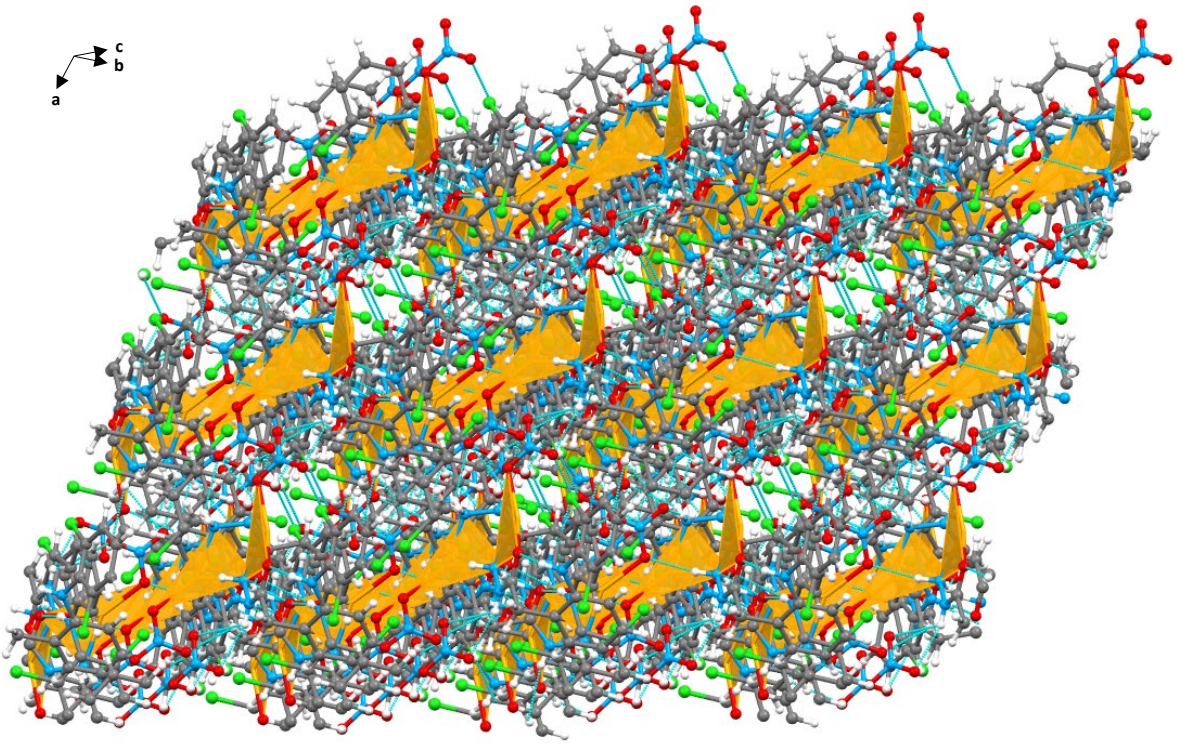

Fig. S14 3D Perspective structure of complex **1**, shaped like peafowl in the nest.

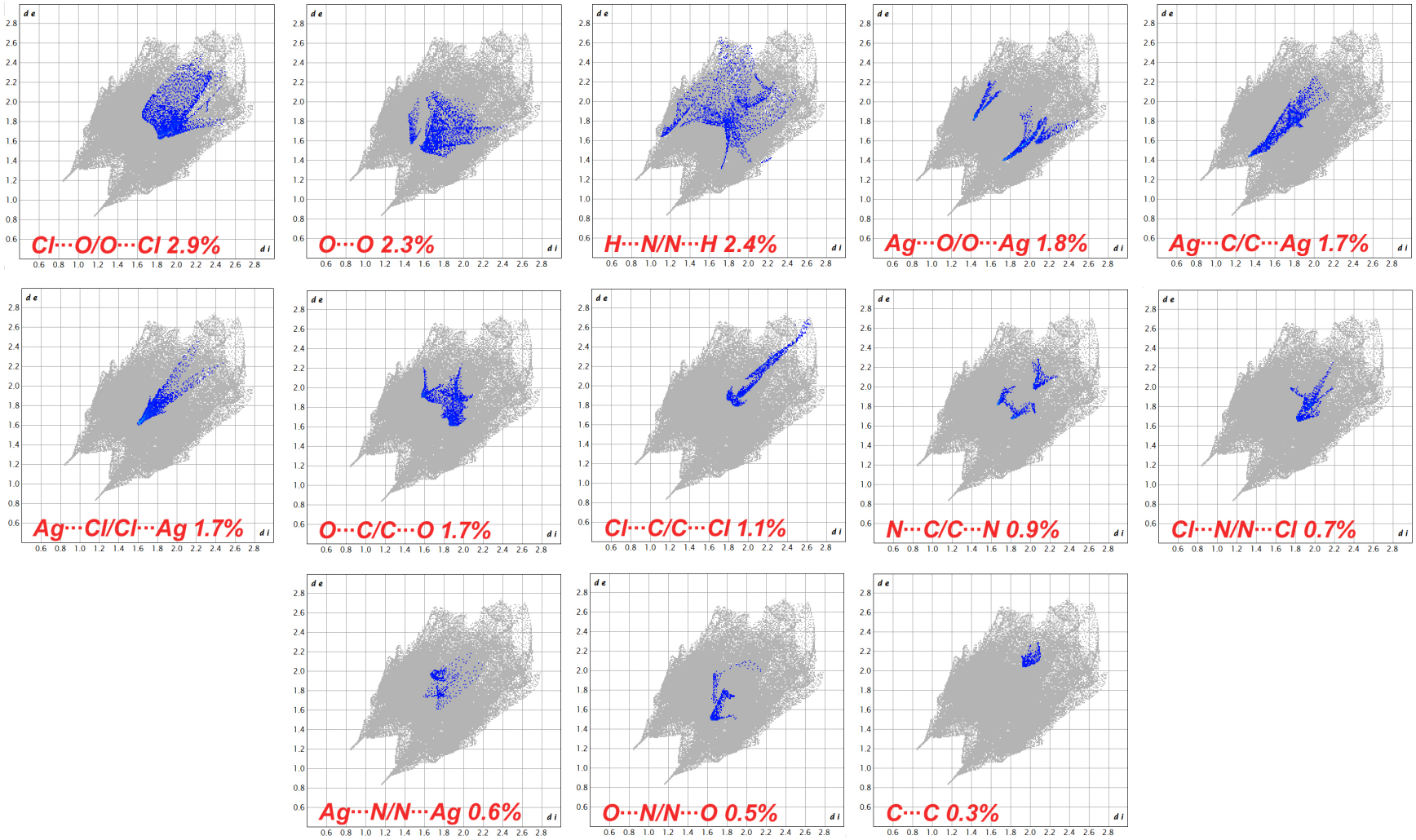

Fig. S15 2D fingerprint plots of complex **1** displaying percent contribution of minor intermolecular contacts from HSA.

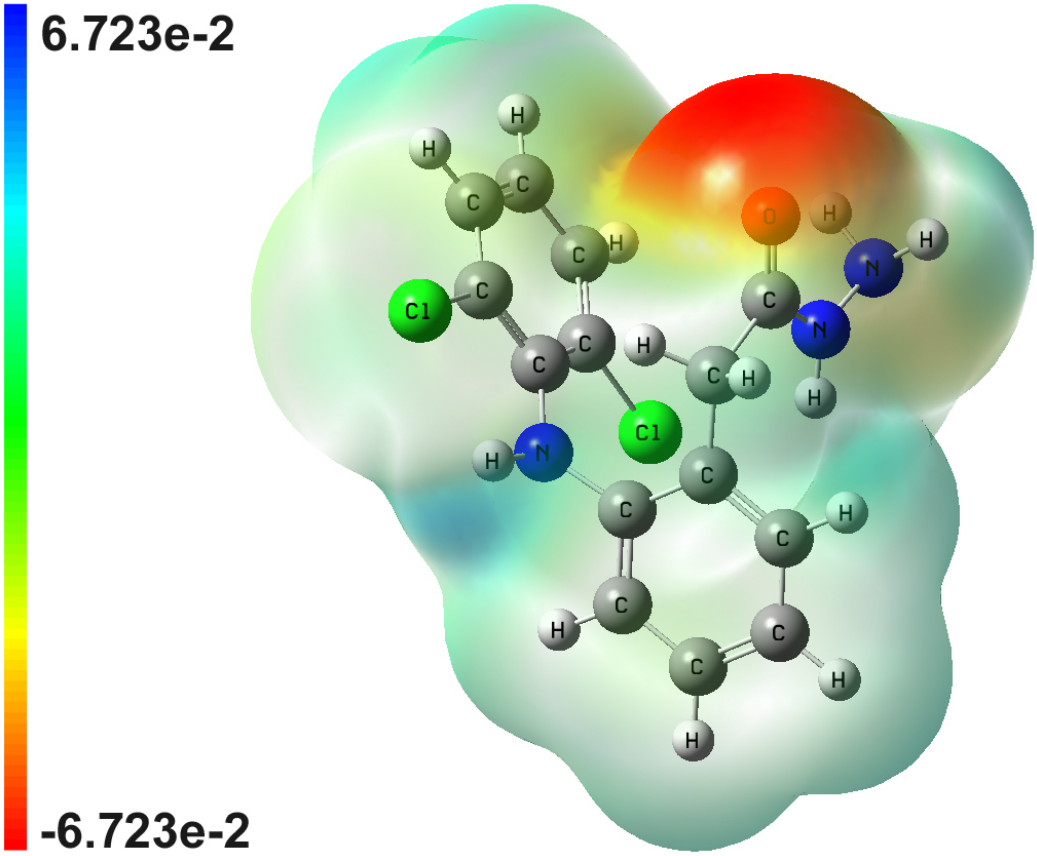

Fig. S16 Molecular electrostatic potential (MEP) map of **dh** ligand.

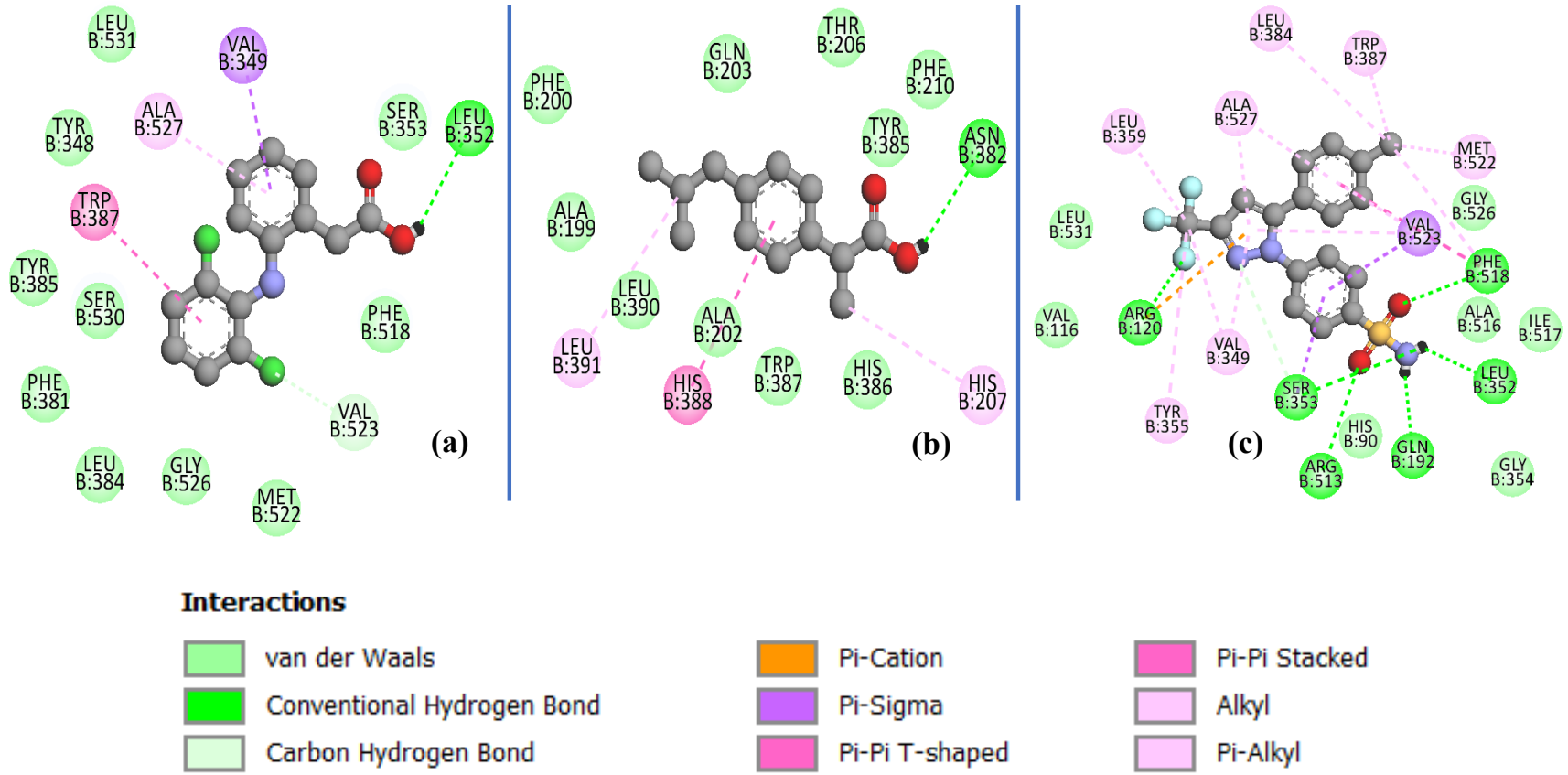

Fig. S17 2D docking interactions of reference anti-inflammatory drugs, (a) diclofenac, (b) ibuprofen, and (c) celecoxib, in the binding pocket of human COX-2 protein (PDB ID: 5kir).

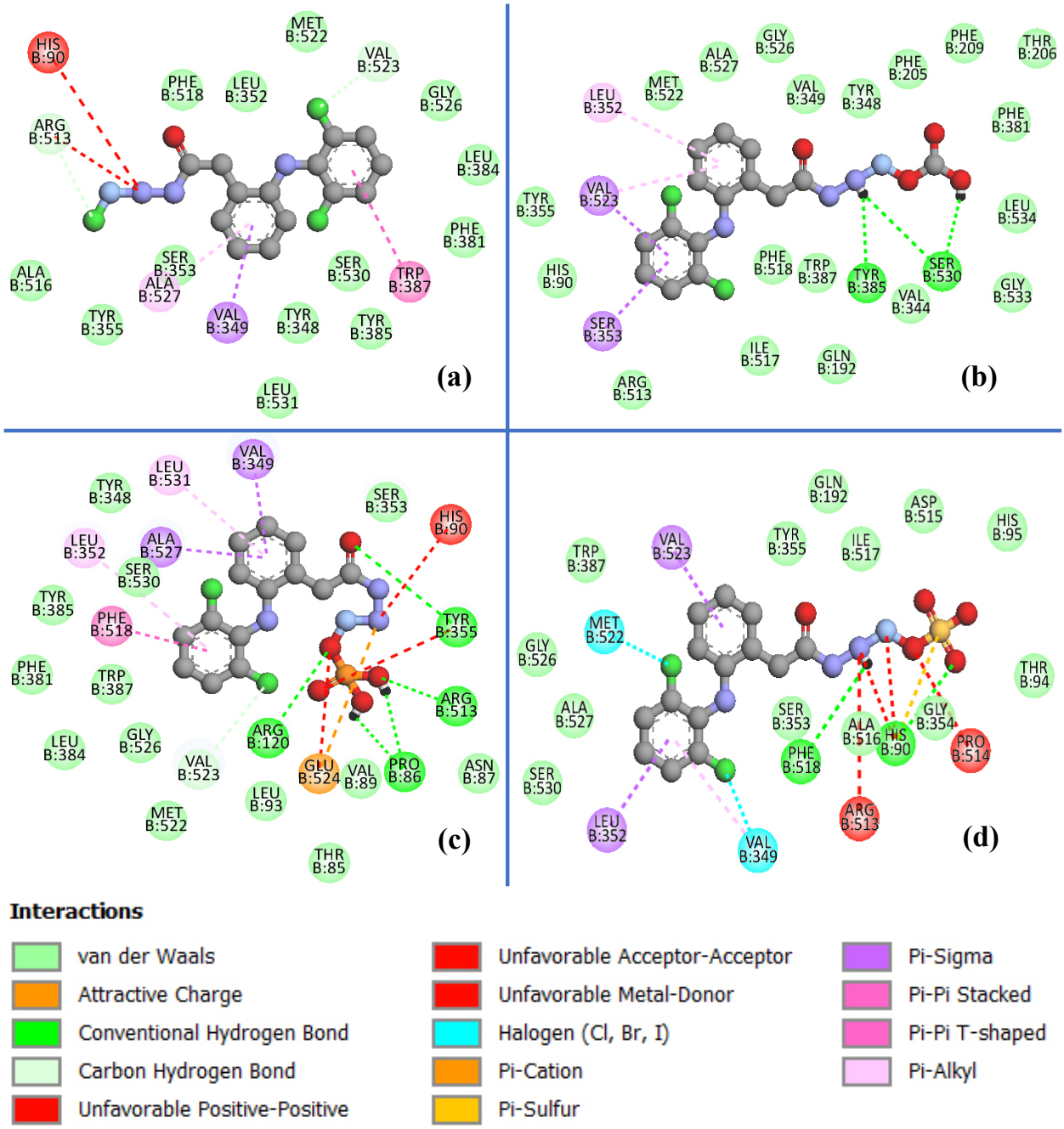

Fig. S18 2D docking interactions of anion exchanged complex **1** in the binding pocket of human COX-2 protein (PDB ID: 5kir), where nitrate is substituted with bio-monoanions (a) Cl^-, (b) HCO_3^-, (c) $H_2PO_4^-$, and (d) HSO_4^-.

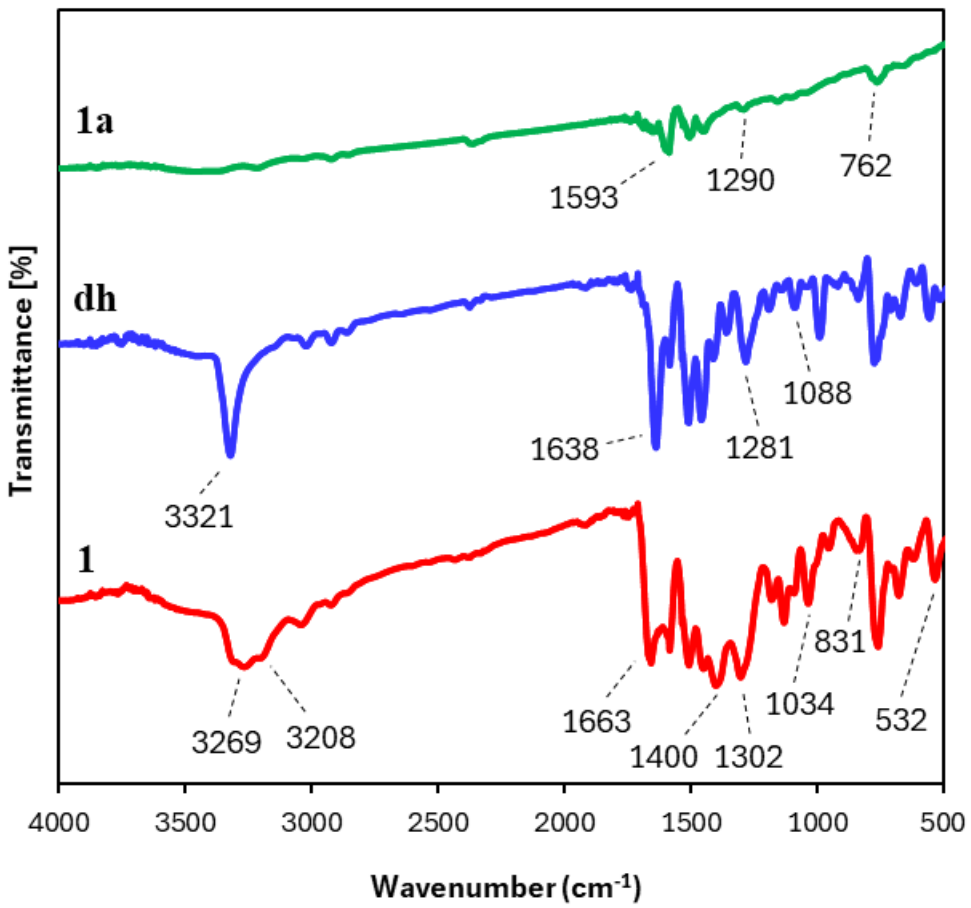

Fig. S19 FT-IR spectrum of silver NPs (**1a**), in comparison with precursor **dh** (ligand and reducing agent) and co-product complex **1**. The disappearance of hydrazinic amine bands and a considerable shift in carbonyl band for **1a** relative to **dh** suggests **dh** oxidation into diclofenac (respective carboxylic acid) and formation of diclofenac-capped Ag NPs.

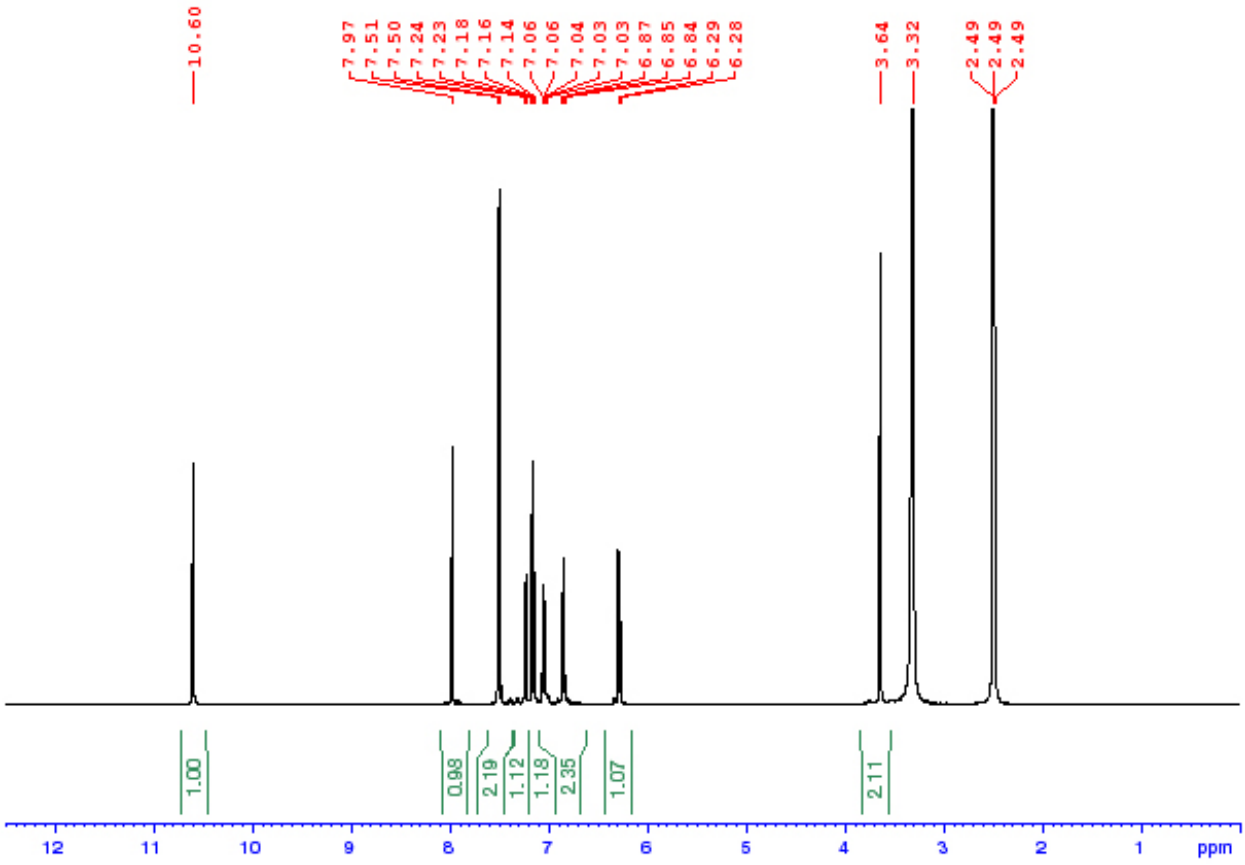

Fig. S20 ^{1}H NMR spectrum of silver NPs (**1a**) in fresh DMSO solution at 500 MHz. Absence of hydrazinic NH and NH_2 proton peaks, appearance of a new peak for -COOH proton at 10.6 ppm, and significant shift in the signal for protons of Ar-NH-Ar (7.97 ppm) and CH_2 (3.64 ppm) relative to precursor **dh** (ligand and reducing agent) suggests **dh** oxidation into diclofenac (respective carboxylic acid) and formation of diclofenac-capped Ag NPs.

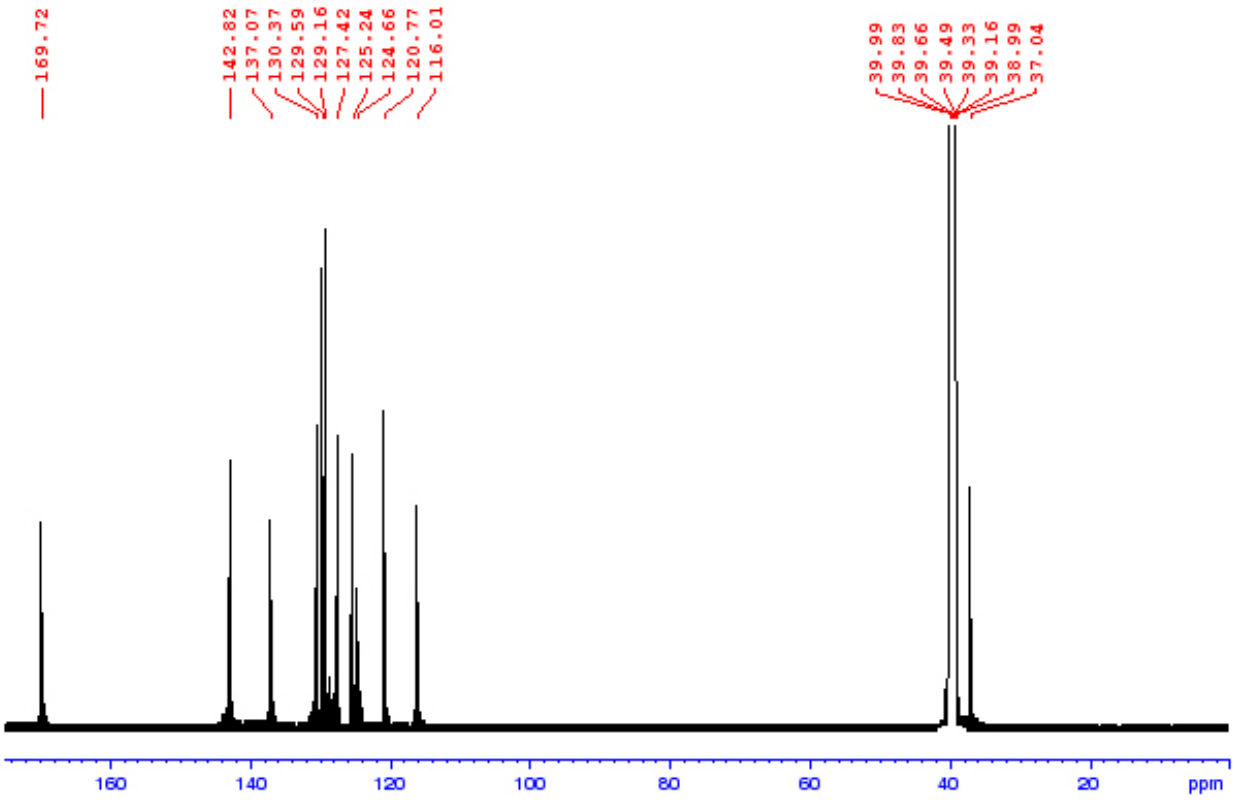

Fig. S21 $^{13}C\{^{1}H\}$ NMR spectrum of silver NPs (**1a**) in fresh DMSO solution at 125 MHz. A considerable upfield shift in the signal for carbonyl carbon (169.72 ppm) and CH_2 (37.04 ppm) relative to precursor **dh** (ligand and reducing agent) suggests **dh** oxidation into diclofenac (respective carboxylic acid) and formation of diclofenac-capped Ag NPs.

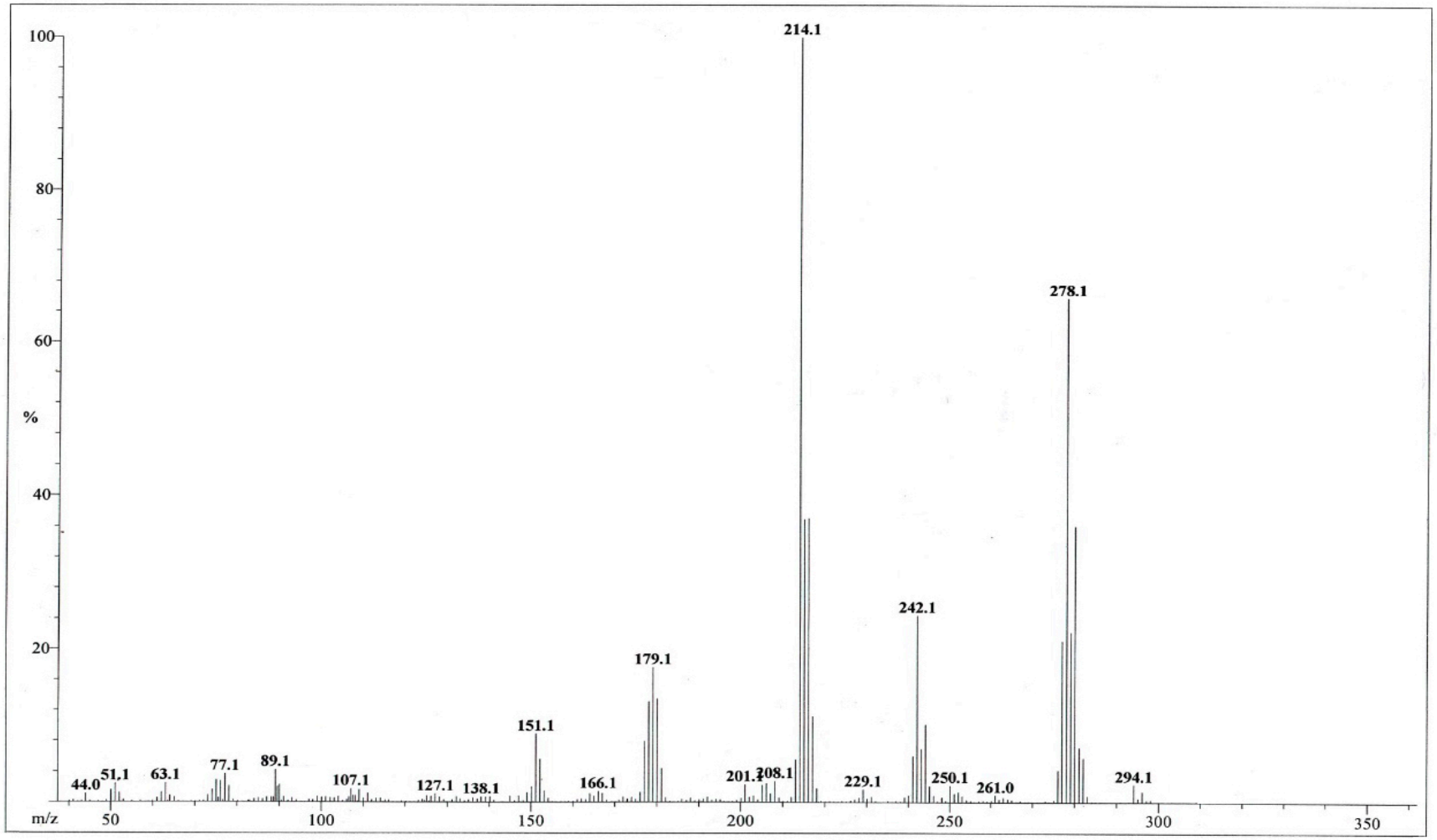

Fig. S22 EI-MS spectrum of silver NPs (**1a**). The peak at *m*/*z* = 294 corresponds to molecular ion $[M-1]^+$ of diclofenac acid (**da**), the oxidized product of **dh**, coated on Ag NPs. The peaks for silver^0 clusters or attached molecules or fragments were not observed, probably due to their charge neutrality or instability.

Table S1 Summarized crystal data and structure refinement specifications for complex **1**

Crystal data			
Chemical Formula	$C_{28}H_{26}Ag_2Cl_4N_8O_8$	Unit cell dimensions	a = 8.9484(4) Å
Fw (g mol^{-1})	960.11		b = 10.7265(4) Å
Crystal system	triclinic		c = 19.5888(8) Å
Space group	P-1		α = 91.661(2)°
Crystal size (mm^3)	0.120 x 0.140 x 0.240		β = 102.5380(10)°
T (K)	273(2)		γ = 107.355(2)°
λ (Å)	1.54178 Å	D_{calcd} (g cm^{-3})	1.829
V (Å^3)	1742.95(13)	μ (mm^{-1})	12.360
Z	2	F(000)	952
Data collection and structure refinement			
θ range (°)	2.32–68.50	Max./min. transmission	0.3190/0.1550
Index ranges	$-10 \le h \le 10$	Data/restraints/parameters	6379/0/462
	$-12 \le k \le 12$	Goodness-of-fit on F^2	1.054
	$-23 \le l \le 23$	Final R indices [I > 2σ(I)]	R_1 = 0.0524, wR_2 = 0.1438[a]
Reflections collected	45076	R indices (all data)	R_1 = 0.0572, wR_2 = 0.1515
Independent reflections	6379 [R_{int} = 0.0626]	Extinction coefficient	0.0055(3)
Completeness	99.6% (to θ = 68.50°)	Largest diff. peak and hole	1.507 and –1.323 eÅ^{-3}

[a] $w = 1/[\sigma^2(F_o^2) + (0.0871P)^2 + 2.7804P]$, where $P = (F_o^2 + 2F_c^2) / 3$.

Table S2 Selected bond lengths and angles from X-ray crystallographic data of complex **1**

Bond parameters			
Bond lengths (Å)			
Ag1-N2	2.255(5)	Ag1′-N2′	2.294(5)
Ag1-O1	2.485(3)	Ag1′-O1′	2.386(4)
Ag1-O2	2.190(5)	Ag1′-O2′	2.242(3)
N1-C1	1.327(4)	N1′-C1′	1.324(6)
N1-N2	1.409(5)	N1′-N2′	1.403(5)
N3-C8	1.419(6)	N3′-C8′	1.404(6)
N3-C9	1.411(5)	N3′-C9′	1.379(9)
O1-C1	1.236(5)	O1′-C1′	1.234(6)
O2-N4	1.265(5)	O2′-N4′	1.249(6)
O3-N4	1.227(6)	O3′-N4′	1.234(5)
O4-N4	1.224(5)	O4′-N4′	1.239(5)
Bond angles (°)			
N2-Ag1-O2	143.3(1)	N2′-Ag1′-O2′	130.2(1)
N2-Ag1-O1	69.9(1)	N2′-Ag1′-O1′	71.2(1)
O2-Ag1-O1	142.3(1)	O2′-Ag1′-O1′	145.5(1)

Table S3 Hirshfeld contact surfaces, random contacts and enrichment ratios for complex **1** crystal

	H	C	N	O	Cl	Ag
Contacts (%)						
H	15.2	-	-	-	-	-
C	15.3	0.3	-	-	-	-
N	2.4	0.9	0	-	-	-
O	30.7	1.7	0.5	2.3	-	-
Cl	15.9	1.1	0.7	2.9	0	-
Ag	4.3	1.7	0.6	1.8	1.7	0
Surface%	49.5	10.7	2.6	21.1	11.2	5.1
Random contacts (%)						
H	24.5	-	-	-	-	-
C	10.5	1.1	-	-	-	-
N	2.5	0.5	0.1	-	-	-
O	20.9	4.5	1.1	4.5	-	-
Cl	11.0	2.4	0.6	4.7	1.2	-
Ag	5.0	1.1	0.3	2.1	1.1	0.3
Enrichment Ratios (E_{XY})						
H	0.62	-	-	-	-	-
C	1.45	0.26	-	-	-	-
N	0.95	1.66	0.0	-	-	-
O	1.47	0.38	0.46	0.52	-	-
Cl	1.44	0.46	1.23	0.62	0.0	-
Ag	0.86	1.58	2.33	0.84	1.51	0.0

Table S4 AIM topological parameters at (3, -1) bond critical points of molecular interactions in complex **1**

Interactions	**BCPs**	***ρ*** **(au)**	***G*** **(au)**	***V*** **(au)**	***H*** **(au)**	$\nabla^2\rho$ **(au)**	$\lvert V\rvert/G$	E_{int} **(kcal mol^{-1})**
Intramolecular								
Ag1···N2	*a*	0.0665	0.0886	-0.1013	-0.0127	0.3037	1.143	31.78
Ag1′···N2′	*a′*	0.0612	0.0808	-0.0913	-0.0105	0.2813	1.130	28.64
Ag1···O2	*b*	0.0661	0.0974	-0.1060	-0.0086	0.3555	1.088	33.26
Ag1′···O2′	*b′*	0.0295	0.0850	-0.0909	-0.0059	0.3162	1.069	28.51
Ag1···O1	*c*	0.0175	0.0429	-0.0420	0.0009	0.1752	0.979	13.18
Ag1′···O1′	*c′*	0.0430	0.0577	-0.0587	-0.0010	0.2269	1.017	18.43
N3-H3···O1	*d*	0.0107	0.0105	-0.0074	0.0030	0.0540	0.708	2.32
N3′-H3′···O1′	*d′*	0.0124	0.0123	-0.0092	0.0030	0.0612	0.752	2.89
Cl1···O1	*e*	0.0052	0.0041	-0.0031	0.0009	0.0200	0.773	0.99
Cl1′···O1′	*e′*	0.0046	0.0035	-0.0027	0.0008	0.0173	0.775	0.86
Cl1···O4	*f*	0.0035	0.0027	-0.0020	0.0007	0.0136	0.743	0.63
Cl1′···O4′	*f′*	0.0017	0.0013	-0.0009	0.0004	0.0070	0.706	0.30
Intermolecular								
N2′-H2A′···O2	*g*	0.0175	0.0166	-0.0143	0.0023	0.0757	0.861	4.49
Ag1′···O3	*h*	0.0069	0.0048	-0.0040	0.0009	0.0227	0.823	1.25
N2-H2B···O3	*i,i′*	0.0161	0.0146	-0.0125	0.0021	0.0671	0.855	3.93
Ag1···O2	*j, j′*	0.0052	0.0033	-0.0029	0.0004	0.0145	0.893	0.92
Ag1′···$\pi_{(cg1)}$	*k*	0.0218	0.0174	-0.0175	-0.0001	0.0695	1.003	5.48
N2′-H2B′···O1	*l*	0.0105	0.0098	-0.0074	0.0024	0.0489	0.754	2.32
C4H4···O4′	*m*	0.0074	0.0062	-0.0043	0.0019	0.0325	0.691	1.35
N1···O2′	*n*	0.0052	0.0037	-0.0028	0.0009	0.0183	0.752	0.86
Ag1′···N1	*o*	0.0050	0.0029	-0.0025	0.0004	0.0134	0.864	0.80
C6H6···$\pi_{(cg1')}$	*p*	0.0039	0.0026	-0.0014	0.0012	0.0154	0.537	0.44
C5-H5···Cl1′	*q*	0.0030	0.0021	-0.0013	0.0009	0.0120	0.602	0.41
C7H7···$\pi_{(cg1')}$	*r*	0.0027	0.0016	-0.0009	0.0007	0.0093	0.554	0.28
N2′-H2B′···Cl1	*s*	0.0021	0.0015	-0.0009	0.0006	0.0085	0.604	0.29
N3′···$\pi_{(cg1)}$	*t*	0.0017	0.0010	-0.0007	0.0003	0.0049	0.727	0.22

Table S5 Comparison of anti-inflammatory profile of complex **1** with some earlier reported silver compounds

Ag compounds	**Assay applied**	**Concentration (μg mL^{-1})**	**% Activity**	**IC$_{50}$ (μg mL^{-1})**	**Standard (% activity, IC$_{50}$)**	**Ref.**
Complex **1**	intracell ROS inhibition	25	91	2.6	Diclofenac (73%, 8.3 μg mL^{-1})	This work
Ag^{I} *N*-heterocyclic carbene	intracell IL-1 inhibition	303.8	60	148.9	Indomethacin (68%)	1
	intracell TNF-α inhibition		55	275.6	Indomethacin (73%)	
	intracell NO inhibition		20	> 1519	Indomethacin (81%)	
Ag^{I}-ibuprofen-caffeine	COX-1 inhibition	-	-	62.5	-	2
	COX-1 inhibition	-	-	26.5	-	
Ag^{I}-naproxen	RBC membrane stabilization	100	55	-	Naproxen (69%)	3
Ag^{I}-phosphine-chlorothioamide	Anti-burn activity in animals	197 (1.7 ml/day for 20 days)	51	-	-	4
Ag^{I}-3-py-ibuprofen xerogel	intracell prostaglandin-E$_2$ inhibition	-	82	-	Ibuprofen (83%)	5
Ag nanoparticles (*A. elatus*)	albumin anti-denaturation	100	67	47.3	Aspirin (79%, 68.8 μg mL^{-1})	6
	RBC membrane stabilization		74	55.9	Aspirin (86%, 65.0 μg mL^{-1})	

Table S6 COX-2 (5kir) molecular docking interactions and binding energy data for **dh** and its complexes

Compound	Docking score (kcal mol^{-1})	Binding sites	Interaction type[a]	Distance (Å)
dh	−11.50	Lig:H23-Gln192:OE1	HB	2.17
		Lig:H23-Leu352:O	HB	2.80
		Lig:H24-Ser353:O	HB	2.77
		Trp387-Lig	HP (π-π, T)	5.91
		Trp387-Lig	HP (π-π, T)	4.77
		Lig-Val349	HP (π-alkyl)	4.81
		Lig-Leu352	HP (π-alkyl)	4.97
		Lig-Ala527	HP (π-alkyl)	5.16
Complex **1**	−12.57	His90:NE2-Lig:O3	ES (attractive)	5.50
		His90:NE2-Lig:O4	ES (attractive)	5.09
		Arg513:NH1-Lig:O3	ES (attractive)	3.91
		Arg513:NH1-Lig:O4	ES (attractive)	4.95
		Phe518:HN-Lig:O4	HB	2.47
		Arg513:CD-Lig:O2	HB	2.85
		Arg513:CD-Lig:O3	HB (C)	2.94
		Val523:CA-Lig:Cl2	HB (C); Halogen	3.20
		Lig:N4-His90	ES (π-cation)	4.99
		Val349:CG1-Lig	HP (π-σ)	3.35
		Trp387-Lig	HP (π-π, T)	4.82
		Lig-Ala527	HP (π-alkyl)	3.92
Complex **2**	−10.91	Lig:Zn18-Glu524:OE1	ES (attractive)	3.84
		Lig:N23-Glu524:OE1	ES (attractive)	5.53
		Arg120:HH22-Lig:O19	HB	2.39
		Lig:O26-Phe470:O	HB	2.71
		Lig:O26-Glu524:O	HB	3.03
		Glu524:OE1-Lig:Cl16	Halogen	3.20
		Arg120:NH1-Lig	ES (π-cation)	3.78
		Val89:CG2-Lig	HP (π-σ)	3.66
		Lig-Val89	HP (π-alkyl)	5.27
		Lig-Val116	HP (π-alkyl)	4.63
		Lig-Arg120	HP (π-alkyl)	5.47
		Lig-Pro86	HP (π-alkyl)	4.70
Diclofenac	−9.78	Lig:H21-Leu352:O	HB	2.21
		Val523:CA-Lig:Cl9	HB (C); Halogen	3.05
		Val349:CG1:Lig	HP (π-σ)	3.40
		Trp387:Lig	HP (π-π, T)	4.90
		Lig-Ala527	HP (π-alkyl)	4.12
Ibuprofen	−9.20	Lig:H12-Asn382:O	HB	2.13
		His388-Lig	HP (π-π, stacked)	4.88
		Lig:C14-Leu391	HP (alkyl)	4.65
		His207:Lig:C8	HP (π-alkyl)	4.38

[a] HB = hydrogen bond, HP = hydrophobic, ES = electrostatic.

Table S7 COX-2 (5kir) molecular docking interactions for celecoxib[a]

Binding Sites	**Distance (Å)**	**Interaction Category[b]**	**Interaction Types**
Arg120:HH12-Lig:F25	2.99	HB;Halogen	Conventional HB;Halogen (F)
Arg513:HH11-Lig:O21	2.79	HB	Conventional HB
Phe518:HN-Lig:O20	2.33	HB	Conventional HB
Lig:H23-Leu352:O	2.12	HB	Conventional HB
Lig:H23-Ser353:O	2.64	HB	Conventional HB
Lig:H24-Gln192:OE1	1.87	HB	Conventional HB
Ser353:CB-Lig:N2	3.44	HB	Carbon HB
Arg513:CD-Lig:O21	3.31	HB	Carbon HB
Arg120:NH1-Lig	4.91	ES	Pi-Cation
Ser353:CA-Lig	3.51	HP	Pi-Sigma
Val523:CG1-Lig	3.93	HP	Pi-Sigma
Val523:CG2-Lig	3.38	HP	Pi-Sigma
Phe518-Lig	5.59	HP	Pi-Pi Stacked
Lig:C12-Leu384	5.29	HP	Alkyl
Lig:C12-Met522	4.42	HP	Alkyl
Lig:C28-Val349	4.92	HP	Alkyl
Lig:C28-Leu359	4.73	HP	Alkyl
Tyr355-Lig:C28	5.18	HP	Pi-Alkyl
Trp387-Lig:C12	5.29	HP	Pi-Alkyl
Trp387-Lig:C12	4.65	HP	Pi-Alkyl
Phe518-Lig:C12	4.60	HP	Pi-Alkyl
Lig-Val349	4.80	HP	Pi-Alkyl
Lig-Val523	5.44	HP	Pi-Alkyl
Lig-Ala527	4.21	HP	Pi-Alkyl
Lig-Val523	4.85	HP	Pi-Alkyl
Lig-Ala527	4.69	HP	Pi-Alkyl

[a] Free binding energy = −14.36 kcal mol^{-1}.

[b] HB = hydrogen bond, HP = hydrophobic, ES = electrostatic.

TABLE S8 COX-2 (5kir) molecular docking interactions and binding energy data for complex **1** after exchange of its nitrate with other bio-monoanions

Exchanged monoanions	Docking score (kcal mol^{-1})	Binding sites	Interaction type[a]	Distance (Å)
Cl^-	−10.07	Arg513:CD-Lig:Cl26	HB (C)	3.74
		Val523:CA-Lig:Cl9	HB (C); Halogen	3.29
		Val349:CG1-Lig	HP (π-σ)	3.35
		Trp387-Lig	HP (π-π, T)	5.99
		Trp387-Lig	HP (π-π, T)	4.86
		Lig-Ala527	HP (π-alkyl)	4.05
HCO_3^-	−12.73	Lig:H24-Tyr385:OH	HB	2.19
		Lig:H24-Ser530:OG	HB	2.89
		Lig:H30-Ser530:O	HB	2.13
		Ser353:CA-Lig	HP (π-σ)	3.53
		Val523:CG1-Lig	HP (π-σ)	3.81
		Val523:CG2-Lig	HP (π-σ)	3.35
		Lig-Leu352	HP (π-alkyl)	5.31
		Lig-Val523	HP (π-alkyl)	4.49
$H_2PO_4^-$	−12.11	Lig:N6-Glu524:OE2	ES (attractive)	5.24
		Arg120:HH21-Lig:O10	HB	2.17
		Tyr355:HH-Lig:O3	HB	2.80
		Arg513:HH12-Lig:O15	HB	2.31
		Arg513:HH22-Lig:O15	HB	2.05
		Lig:H14-Pro86:O	HB	1.97
		Lig:H16-Pro86:O	HB	1.99
		Val523:CA-Lig:Cl25	HB (C); Halogen	3.12
		Val349:CG1-Lig	HP (π-σ)	3.30
		Ala527:CB-Lig	HP (π-σ)	3.63
		Phe518-Lig	HP (π-π, stacked)	5.45
		Lig-Leu531	HP (π-alkyl)	5.13
		Lig-Leu352	HP (π-alkyl)	5.44
$HSO4^-$	−11.94	His90:HE2-Lig:O28	HB	2.98
		Lig:H24-Phe518:O	HB	2.85
		Val349:O-Lig:Cl9	Halogen	3.06
		Met522:O-Lig:Cl10	Halogen	3.09
		Lig:N22-His90	ES (π-cation)	4.17
		Leu352:CD1-Lig	HP (π-σ)	3.88
		Val523:CG1-Lig	HP (π-σ)	3.56
		Val523:CG2-Lig	HP (π-σ)	3.52
		Lig:S29-His90	π-S	4.61
		Lig-Val349	HP (alkyl)	5.13

[a] HB = hydrogen bond, HP = hydrophobic, ES = electrostatic.

References

1 M. A. Iqbal, M. I. Umar, R. A. Haque, M. B. K. Ahamed, M. Z. B. Asmawi, and A. M. S. A. Majid, *J. Inorg. Biochem.*, 2015, **146**, 1–13.

2 A. Borowka, A. Sieroslawska, A. Baier, A. Rymuszka, and E. Olszewska, *Molecules*, 2024, **29**, 506.

3 M. S. Hasan, and N. Das, *Alex. J. Med.*, 2017, **53**(2), 157–165.

4 L. Kyros, N. Kourkoumelis, M. Kubicki, L. Male, M. B. Hursthouse, I. I. Verginadis, E. Gouma, S. Karkabounas, K. Charalabopoulos, and S. K. Hadjikakou, *Bioinorg. Chem. Appl.*, 2010, **2010**, 386860.

5 K. Sarkar, S. Khasimbi, S. Mandal, and P. Dastidar, *ACS Appl. Mater. Interfaces*, 2018, **10**(36), 30649–30661.

6 B. V. Kumari, R. Mani, B. R. Asokan, K. Balakrishnan, A. Ramasamy, R. Parthasarathi, C. Kandasamy, R. Govindaraj, N. Vijayakumar, and S. Vijayakumar, *J. Compos. Sci.*, 2023, **7**, 453.